Action mechanism of a novel agrichemical quinofumelin against *Fusarium graminearum*

Qian Xiu [a,1], Xiaoru Yin [a,1], Yuanyuan Chen [b,1] Ziyang Zhang [a], Yushuai Mao [a], Tianshi Wang [b], Jie Zhang [a], Mingguo Zhou [a,2], Yabing Duan [a,2]

[a] College of Plant Protection, Nanjing Agricultural University, Nanjing 210095, China.

[b] College of Science, Nanjing Agricultural University, Nanjing 210095, China.

[1] Qian Xiu, Xiaoru Yin and Yuanyuan Chen contributed equally to this work.

[2] Corresponding author: E-mail address: mgzhou@njau.edu.cn (Mingguo Zhou); dyb@njau.edu.cn (Yabing Duan)

Abstract

Modern fungicides have made significant contributions to crop disease management, but the development of resistant fungal strains has caused their failure in disease control. Therefore, developing fungicides with novel action mechanisms is the most effective measure to manage resistance. Quinofumelin, a novel quinoline fungicide, exhibits exceptional antifungal activity against phytopathogens. However, there is currently no available information on its mechanism of action. Here, we used transcriptome and metabolome analysis to observe a co-enrichment pattern of differentially expressed genes (DEGs) and differentially accumulated metabolites (DAMs) within pyrimidine biosynthesis pathway (PBP), identifying down-regulation of dihydroorotate dehydrogenase (DHODH). Exogenous UMP, uridine or uracil (metabolites in PBP) successfully restored quinofumelin-induced inhibition of mycelial growth in *Fusarium graminearum* and *Fusarium asiaticum*. Additionally, the deletion of *FgDHODHII* was determined to be lethal; however, mycelial growth of ΔFgDHODHII mutants could be restored by adding UMP, uridine or uracil. These findings indicate that the deficiencies in *FgDHODHII* are functionally equivalent to complete inhibition of its activity by quinofumelin. Finally, molecular docking, surface plasmon resonance (SPR) and microscale thermophoresis (MST) results strongly support the precise interaction between quinofumelin and FgDHODHII. Collectively, these findings provide compelling evidence for the involvement of *de novo* uracil biosynthesis as mechanism of action for quinofumelin while identifying FgDHODHII as its specific target.

Key words: Action mechanism; Fungicide target; Quinofumelin; *Fusarium graminearum*

Introduction

Agrochemical fungicides have a history spanning over 3000 years in the control of plant diseases, and have undergone a development process from traditional protective fungicides with multiple action sites to modern selective fungicides with single action site[1]. The introduction of the first fully systemic seed treatment agent (carboxin, a succinate dehydrogenase inhibitor) in 1966 and the launch of the first broad-spectrum foliar systemic fungicide (benomyl, a tubulin polymerization inhibitor) in 1968 represent significant milestones in the advancement of modern selective fungicides with single action site[2-3]. Owing to their exceptional selectivity, potent activity, specific target site, and low toxicity, modern selective fungicides have gained widespread acceptance and witnessed an increasing market share year after year. However, like every coin has two sides, these types of fungicides encounter substantial challenges related to serious resistance issues when deployed in agricultural fields. Numerous reports have been published on plant pathogens developing resistance to modern selective fungicides, which often result in failures or reductions in the effectiveness of chemical control against plant diseases and lead to decreased crop yields and

quality (https://www.frac.info/)[4-6]. Therefore, it is crucial to expedite the development of new-generation selective fungicides with innovative modes of action. Based on a single fungicide target, numerous modern selective fungicides can be developed. For instance, 24 commercialized available fungicides have been created so far based on the respiratory chain complex II as the target. Similarly, another 20 commercialized fungicides have been developed targeting the respiratory chain complex III. Additionally, there are already 37 commercialized fungicides that specifically target the fungicide target C14-demethylase in ergosterol biosynthesis (https://www.frac.info/). Therefore, discovering novel targets poses a significantly greater challenge compared to creating new fungicides within the existing categories.

According to the latest information released by the Fungicide Resistance Action Committee (FRAC), over 30 fungicide selective targets have been identified and acknowledged in the field of fungicide biological research spanning more than 130 years. Currently, these targets have been identified based on the successful development of fungicides and are all related proteins that are essential for pathogen growth or pathogenicity. Extensive identification and functional analysis of essential genes for growth or pathogenicity in plant pathogens have been achieved with rapid advancements in molecular biology techniques; however, there is no precedent for successfully developing commercialized fungicides targeting genes involved in growth or pathogenicity. The creation of highly active modern selective fungicides currently relies on the structural characteristics of existing targets and is accomplished through technologies such as AI drug discovery and design (AIDD), and computer aided drug design (CADD). The biological functions of drug targets are highly conserved, although variations may occur at critical amino acid sites during genetic evolution. Therefore, it is crucial to explore drug targets and analyze their structural characteristics in order to develop novel fungicides with enhanced activity and selectivity. Recently, the Fungicide Biology group from Nanjing Agricultural University proposed a new concept for targeting pesticides based on the principles of targeted medicine. The objective is to create specialized targeted pesticides that exhibit higher activity, greater selectivity, stronger specialization, lower toxicity, and environmental friendliness by leveraging the structural characteristics of pesticide targets. This approach aims to provide essential technical support for scientifically controlling crop diseases.

Quinofumelin (CAS 861647-84-9) is a novel quinoline fungicide developed by Mitsui Chemicals Co., Ltd. Japan. Due to their significant bioactivity, quinoline compounds and their derivatives have found extensive applications in medicine and pesticides[7-9]. Based on their biological and physiological characteristics, quinolines are classified as FRAC group 13 (https://www.frac.info/). However, the precise mode of action of quinolines against plant pathogens remains unclear. In addition, quinofumelin exhibits no cross-resistance to currently extensively used fungicides, indicating its unique action target against phytopathogenic fungi. Therefore, this study unveils that the mechanism of action for quinofumelin involves *de novo* synthesis of uracil that identifies dihydroorotate dehydrogenase as its specific target. This newly discovered selective target for antimicrobial agents provides a valuable resource for the design and development of targeted pesticides.

Results

Transcriptomic analysis of *F. graminearum* as affected by quinofumelin

To evaluate the quality of RNA-Seq data, we conducted a comprehensive analysis for quality control. In the principal component analysis, PC1 and PC2 accounted for 45.59% and 16.98% of the total variance, respectively. The distinct separation observed between the groups indicates significant differences in gene expression between the controls and experimental samples, which could be used

for subsequent investigations (Supporting Information, Fig. S1). The clustering heat map effectively categorized the controls and experimental samples into distinct clusters based on their gene expression profiles, demonstrating robust biological replication with minimal intra-group variability and ensuring the reliability of the data. Moreover, notable inter-group dissimilarities highlighted variations among different treatment samples (Fig. 1c).

The differential analysis unveiled a total of 234 significantly differentially expressed genes (DEGs) between the control and experimental samples. Among these findings, there were identified as up-regulated for a count of 97 genes while down-regulation was observed in case of another set comprising around 137 genes (Fig. 1a). A graphical representation called "volcano plot" was employed to depict the statistical distribution pattern exhibited by these DEGs (Fig. 1b). To gain deeper insights into gene functionalities, Gene Ontology (GO) and Kyoto Encyclopedia of Genes and Genomes (KEGG) enrichment analysis were performed on these DEGs. The results showed that they are notably enriched in seventeen distinct GO terms spanning across two major categories; eleven molecular functions along with six processes (Fig. 1d). Furthermore, the enrichment analysis highlighted significant associations with various functional attributes including transition metal ion binding, oxidoreductase activity, modified amino acid binding, amide binding, monooxygenase activity, and heme binding. Moreover, the enriched biological processes primarily involved transcriptional regulation driven by nucleic-enabled mechanisms as well as monocarboxylic acid metabolism and RNA biosynthesis. Additionally, the KEGG enrichment analysis identified specific pathways associated with thiamine metabolism, tryptophan metabolism, nitrogen metabolism, amino acid sugar and nucleotide sugar metabolism, pantothenic acid and CoA biosynthesis, as well as nucleotide sugar production compound synthesis (Fig. 1e).

Metabolomic analysis of *F. graminearum* as affected by quinofumelin

In metabolomics principal component analysis, the contribution rate of PC1 was determined to be 76.6% in positive ion mode and 51.2% in negative ion mode, respectively. Moreover, the quality control (QC) samples exhibited highly concentrated results, indicating excellent instrument stability and remarkable data repeatability. Furthermore, a distinct separation between groups was observed, particularly prominent in the positive ion mode, indicating significant variations in metabolites among different groups that warrant further investigation (Supporting Information, Fig. S2a and S2b). The findings from Pearson correlation analysis were consistent with those obtained from principal component analysis (Supporting Information, Fig. S2c and S2d). Strong correlations were identified within samples belonging to the same group, while weak correlations were observed between different groups.

Metabolomics analysis revealed a total of 713 differential metabolites, with 14 up-regulated and 699 down-regulated in the positive ion mode, as well as 230 differential metabolites, including 103 up-regulated and 127 down-regulated in the negative ion mode (Supporting Information, Fig. 2a and Fig. S3a). Based on the classification of the identified 943 different metabolites, it was observed that amino acids and their derivatives accounted for the highest proportion (17%), followed by organic acids and their derivatives (11%), benzene and substituted derivatives (11%), aldehydes, ketones, esters (11%), and heterocyclic compounds (10%) (Fig. 2c). The volcano plot visually represents the distribution of statistical differences in metabolite abundance between the two groups (Supporting Information, Fig. 2b and Fig. S3b).

KEGG pathways enriched by differential metabolites primarily include arachidonic acid metabolism, pyrimidine metabolism, alanine, aspartate and glutamate metabolism, purine metabolism, citrate cycle, arginine and proline metabolism, fructose and mannose metabolism,

nitrogen metabolism, and metabolic pathways (Fig. 2d). The classification of enrichment pathways for differential metabolites revealed that the majority of these metabolites were associated with nucleotide metabolism (25%), amino acid metabolism (25%), carbohydrate metabolism (25%), and energy metabolism (12.5%) (Supporting Information, Fig. S3c).

Conjoint analysis of transcriptome and metabolome integration

Through transcriptome and metabolome data analysis, we observed a co-enrichment of differentially expressed genes and differentially accumulated metabolites in the pyrimidine metabolism pathway. In the expression calorigrams of metabolites and genes depicting the *de novo* biosynthesis pathway of pyrimidine, we identified down-regulation of dihydroorotate dehydrogenase (DHODH) in the experimental groups. This down-regulation hinders the conversion of dihydroorotate to orotate, thereby inhibiting the biosynthesis of downstream metabolites orotidine-5P and uracil, leading to their decreased abundance (Fig. 2e). Thus, we conclude that the action mechanism of quinofumelin may involve inhibition of the *de novo* biosynthesis pathway of pyrimidine.

Identification of DHODHII in *F. graminearum*

The *FgDHODHII* sequences in *F. graminearum* were identified by performing a BLAST search against the National Center for Biotechnology Information (NCBI) GenBank database, using *Homo sapiens* DHODHII amino acid sequences as a query. *FgDHODHII* is a gene consisting of 1419 bp without introns and is predicted to encode a protein consisting of 472 amino acids. Orthologs of *FgDHODHII* were obtained using the BLAST algorithm. The phylogenetic tree was constructed based on the amino acid sequences of DHODHII homologous protein with Mega X using the neighbor-joining method. Motif pattern information was generated using the MEME suite[10], while functional domain information and protein coordinates were obtained through CD-search[11]. TBtools software was used for visualizing the tree representation[12]. All DHODHII proteins possess the dihydroorotate dehydrogenase domain (Fig. 3), indicating high conservation among fungi. Besides, these orthologs proteins would potentially interact with the fungicide in other pathosystems.

Recovery test of mycelial growth suppressed by quinofumelin in *Fusarium genus*

The mycelial growth of *F. graminearum* PH-1 was significantly inhibited on CZA plates containing quinofumelin at concentrations of 1 μg/mL (Fig. 4). To investigate the potential recovery of mycelial growth by exogenous dihydroorotate, UMP, uridine, or uracil, CZA plates supplemented with quinofumelin were treated with these compounds. Despite the addition of exogenous dihydroorotate at 50 μg/mL failing to restore mycelial growth, the addition of exogenous UMP, uridine or uracil at 50 μg/mL successfully recovered quinofumelin-induced inhibition of mycelial growth. Similar results were observed in other strains of *F. graminearum* or *F. asiaticum* (Fig. 4 and Fig. S4). Thus, it can be concluded that quinofumelin effectively inhibits the pyrimidine biosynthesis pathways.

The absence of *FgDHODHII* is lethal for mycelial growth in *F. graminearum*

To further investigate the biological functions of *FgDHODHII* in *F. graminearum*, we employed a homologous recombination strategy to generate target gene deletion mutants. Through PCR analysis, two putative *FgDHODHII* deletion mutants were successfully identified. The ΔFgDHODHII mutants exhibited distinct phenotypic differences compared to the wild-type progenitor PH-1 and the respective complemented strain (Fig. 5a). These mutants displayed an inability to grow on CZA plate; however, their mycelial growth was restored when supplemented with 50 μg/mL of exogenous UMP, uridine or uracil, while no recovery was observed with 50 μg/mL of exogenous dihydroorotate (Fig. 5b).

Molecular docking

To facilitate the molecular docking process between FgDHODHII and quinofumelin, ten distinct binding models were generated using AutoDockTools-1.5.7 software, each accompanied by its respective binding energies calculation results. The most favorable conformational arrangement was determined based on its relative ranking in terms of the computed binding energy values and subsequently visualized through PyMOL 2.5.4 software (Fig. 6a). Notably, the obtained docking results revealed a robust interaction between FgDHODHII protein and quinofumelin as evidenced by a calculated negative free energy value of -6.8 kcal/mol.

The precise interaction between FgDHODHII and quinofumelin was verified by Surface plasmon resonance analysis

Surface plasmon resonance (SPR) was utilized to evaluate the interaction affinity between quinofumelin and FgDHODHII in this study. The experiment was conducted using a BIAcore T200 (Cytiva) instrument for biomolecular interaction analysis. FgDHODHII was immobilized as the ligand on the chip surface, while quinofumelin continuously flowed through as the analyte solution. Dilute quinofumelin to different concentration gradients (62.5, 32.15, 15.63, 7.81, 3.91 μM), measure the binding energy, and then fit the binding equilibrium dissociation constant (K_d) value (Fig. 6b). The SPR results revealed that quinofumelin exhibited fast-binding and fast-dissociation modes when interacting with the target protein FgDHODHII. The calculated K_D value was determined as 6.606×10^{-6} M, indicating specific binding of quinofumelin to FgDHODHII.

The interaction between FgDHODHII and quinofumelin was confirmed by microscale thermophoresis

In this study, microscale thermophoresis (MST) was further used to evaluate the interaction affinity between FgDHODHII and quinofumelin. The strength of the binding can be inferred from the Kd value. The experiment was conducted using MO.Control v1.6.1 and data analysis was performed using MO.Affinity Analysis v2.3. By introducing a fluorescent label GFP to the FgDHODHII protein while maintaining its concentration constant, non-fluorescent labeled small molecules were diluted into 16 concentration gradients. Subsequently, the protein solution and small molecule diluent were mixed at a ratio of 19:1 before being loaded into the capillary for further analysis in the machine. The MST assay demonstrated that FgDHODHII exhibited specific binding to quinofumelin in vitro, with a dissociation constant (Kd) of 0.471 ± 0.268 μM, whereas no binding was observed with phenamacril which lacks cross-resistance with quinofumelin (Fig. 6c).

Discussion

In over 130 years of research on fungicide biology, more than 30 novel targets for selective fungicides have been identified. Based on these newly discovered targets, over 200 modern selective fungicides have been developed. Consequently, the identification of novel targets for fungicides poses a significantly greater challenge compared to the development of new fungicides. Currently, modern selective fungicides with single action site are widely applied in agricultural practices for crop disease management. However, these specific types of fungicides encounter substantial obstacles associated with resistance issues when deployed in agricultural fields. Numerous studies have extensively documented cases of plant pathogens developing resistance to modern selective fungicides, resulting in failures or reductions in their efficacy against plant diseases and subsequently leading to decreased crop yields and quality[4-6]. For instance, *Botrytis cinerea*, a significant plant pathogenic fungus, has emerged as multi-resistant population that is resistant to all currently used modern selective fungicides. This poses a formidable challenge for the control of crop grey mold disease caused by *B. cinerea*. Therefore, there is an urgent need for the development of new fungicides with novel mechanisms of action to effectively manage multiple resistance.

The novel quinoline, quinofumelin, developed by Mitsui Chemicals Co., Ltd. Japan, has demonstrated remarkable antifungal activity against plant pathogens such as *F. graminearum* and *Sclerotinia sclerotiorum*[7, 13]. Moreover, our research group found that quinofumelin exhibits no cross-resistance to all types of currently used modern selective fungicides. These findings indicate that quinofumelin possesses a distinctive mode of action against plant pathogens. Based on their biological and physiological characteristics, quinolines are classified as FRAC group 13 (https://www.frac.info/). However, the precise mechanism by which quinolines act against plant pathogens remains unclear. In this study, we investigated the mechanism of action of quinofumelin on *F. graminearum* using a combined analysis of transcriptomics and metabolomics. The transcriptome data revealed that DEGs were involved in 'tryptophan metabolism' and 'amino sugar and nucleotide sugar metabolism'. Furthermore, the metabolome data identified DAMs enriched in 'nucleotide metabolism' and 'amino acid metabolism'. Interestingly, we observed a co-enrichment of DEGs and DAMs in the pyrimidine metabolism pathway. Specifically, we identified a down-regulation of dihydroorotate dehydrogenase (DHODH) in the experimental groups, which impeded the conversion of dihydroorotate to orotate. Consequently, this inhibition led to decreased biosynthesis of downstream metabolites orotidine-5P and uracil. Therefore, we conducted an experiment using *F. graminearum* standard strain PH-1 to quantify mycelial growth by supplementing exogenous uracil, which is the end product of the uracil biosynthesis pathway. This was performed in the presence of complete inhibition of mycelial growth caused by quinofumelin. Surprisingly, the addition of exogenous uracil restored the inhibited mycelial growth induced by quinofumelin (Fig. 4). Meanwhile, similar results were successfully verified with four other *F. graminearum* strains and five *F. asiaticum* strains (Fig. 4 and Fig. S4). Based on our depicted pyrimidine biosynthesis pathway (Fig. 2E), we also supplemented other intermediate products such as dihydroorotate, orotate, UMP, and uridine externally. Except for dihydroorotate and orotate, supplementation of exogenous UMP and uridine effectively restored mycelial growth inhibited by quinofumelin as well. These findings strongly support that quinofumelin acts through modulation of the uracil biosynthesis pathway.

As a key enzyme in the *de novo* pyrimidine biosynthesis pathway, DHODH has previously been investigated as a potential target for inhibiting infectious organisms and as an antitumor agent in mammals[14-15]. Inhibiting DHODH can effectively impede the synthesis of DNA, RNA, and glycoproteins, thereby regulating aberrant cell metabolism and proliferation to ultimately achieve therapeutic objectives[16]. Within mammalian cells, DHODH is closely associated with the mitochondrial membrane and plays a pivotal role in the respiratory chain through its interaction with ubiquinone[17]. Here, using amino acid sequences from *Homo sapiens* DHODHII as a reference query, we have identified FgDHODHII (FGSG_09678), a gene comprising of 1419 bp without any introns, which encodes 472 amino acids in *F. graminearum*. FgDHODHII possesses a typical DHOD-2 like domain (NCBI: cd04738) and belongs to class 2 DHODs. Class 2 DHODHs are membrane-bound enzymes, whereas class 1 enzymes are located in the cytosol[18]. The DHODH enzyme catalyzes a unique redox reaction in the *de novo* pyrimidine biosynthesis pathway[19]. The DHOD-2 like domain can bind orotate and flavin mononucleotide (FMN), facilitating the oxidation of dihydroorotate to orotate and the reduction of the FMN cofactor[20]. Based on the aforementioned findings, we have concluded that DHODHII functions as the target of action for quinofumelin against *F. graminearum*. Consequently, we performed a protoplast transformation assay to delete FgDHODHII in *F. graminearum* and further validate the precise target of action for quinofumelin. Typically, most fungicide targets are either lethal genes or essential pathogenic genes. Therefore, it

is plausible that the inactivation of FgDHODHII may be lethal. In our genetic transformation experiment, exogenous uridine was supplemented to successfully obtain deletion mutants of the FgDHODHII gene. Fortunately, two ΔFgDHODHII mutants were successfully obtained. These mutants exhibited an inability to grow on PDA or CZA medium; however, mycelial growth was fully restored upon addition of uridine to the medium (Fig. 5A). Additionally, exogenous supplementation of UMP or uracil effectively restored mycelial growth. However, the supplementation of dihydroorotate to the medium did not alleviate the growth defect observed in ΔFgDHODHII mutants (Fig. 5B). Furthermore, mycelial growth in two ΔFgDHODHII mutants was restored by exogenously adding UMP, uracil or uridine under quinofumelin treatments. These findings indicate that the defects of FgDHODHII are functionally equivalent to complete inhibition of its activity by quinofumelin and further confirm that the mechanism of action for quinofumelin involves *de novo* synthesis of uracil while identifying FgDHODH as its specific target.

Molecular docking is a computational procedure employed to predict the optimal binding orientation of a ligand with its macromolecular target (receptor), thereby forming a stable complex. In concise terms, docking is a molecular modeling technique employed to predict the interaction between a protein (enzyme) and small molecules (ligands). In this study, we conducted molecular docking analysis between quinofumelin and the target protein FgDHODHII. The docking results unveiled a robust affinity between FgDHODHII and quinofumelin. Furthermore, these findings provided additional evidence that the strong affinity of quinofumelin with FgDHODHII disrupts its activity and function.

Surface Plasmon Resonance (SPR) technique is employed for real-time measurement of molecular interactions[21]. The SPR sensor map characterizes intermolecular interaction rates primarily by conveying the kinetic rate constant, while it characterizes the binding level between molecules mainly by conveying the affinity constant[22-23]. In this study, we used SPR technology to measure the binding energy and kinetics between FgDHODHII and quinofumelin. The binding kinetics of FgDHODHII and quinofumelin demonstrated fast-binding and fast-dissociation modes. Soluble FgDHODHII exhibited an ideal affinity (Kd) of 6.606×10^{-6} M with quinofumelin, falling within the suitable range of 10^{-3} M to 10^{-6} M for biomacromolecule-small molecule interactions. Furthermore, the binding affinity between FgDHODHII and quinofumelin was confirmed by a microscale thermophoresis (MST) assay. Therefore, these data strongly support the precise interaction between quinofumelin and its target protein FgDHODHII. This newly discovered selective target for antimicrobial agents offers a valuable resource for the design and development of targeted pesticides.

Unlike many other dehydrogenases that require NAD or NADP as an electron acceptor, DHODH transfers electrons to ubiquinone, which then transfers electrons into respiratory complex III and eventually to oxygen[24]. Thus, the production of orotate in pyrimidine biosynthesis is coupled with the electron transport system and energy production, exerting additional control over nucleotide synthesis and ensuring its coupling to cellular energy metabolism. In the pyrimidine biosynthesis pathway, DHODHII regulates the conversion from dihydroorotate to orotate. Our findings demonstrated that DHODHII is target of action for quinofumelin. A previous study reported that exogenous orotate but not exogenous dihydroorotate recovered mycelial growth inhibited by quinofumelin, indicating that quinofumelin inhibits the formation of orotate in the pyrimidine biosynthesis pathway[25]. However, we observed that the supplementation of orotate to the medium did not alleviate the growth defect of ΔFgDHODHII mutants. Considering the disparity in mycelial growth inhibition between *F. graminearum* and other fungi, our data suggests that a nonclassical two-site ping-pong mechanism is the most suitable model for DHODH as previously reported[14]. In

the classical ping-pong mechanism, DHODH interacts with dihydroorotate and ubiquinol in an identical confirmation, while orotate and ubiquinone combine with an alternative form[26]. However, similar to brequinar sodium inhibiting the activity of DHODH isolated from mammalian sources, FgDHODHII may follow a nonclassical, two-site ping-pong mechanism. In this nonclassical ping-pong mechanism, the two substrates may not share chemical resemblance and therefore do not bind to a single binding site but likely bind to two adjacent sites that facilitate reactant transfer. The precise nature of the interaction between quinofumelin and FgDHODHII may require further elucidation studies.

Materials and methods

Strains, culture conditions and fungicides

F. graminearum sensitive strain PH-1 and 9 wild-type strains (*F. graminearum* and *F. asiaticum*), and the PH-1 deletion mutants ΔFgDHODHII were maintained in Fungicide Biology Laboratory, Nanjing Agricultural University.

The media used in this study included potato dextrose agar (PDA) medium, Yeast extract peptone dextrose (YEPD) medium, Czapek Solution Agar (CZA) medium and LB medium.

Chemical-grade quinofumelin (Mitsui Agricultural Chemical Company of Japan) was prepared with dimethyl sulfoxide at a concentration of 1×10^4 μg/mL and stored at 4°C.

Transcriptomic assay of mycelial growth in *F. graminearum* as affected by quinofumelin

A total of 20 mL of YEPD medium containing 1 mL of conidia suspension (1×10^5 conidia/mL) was incubated with shaking (175 rpm/min) at 25°C. After 24 h, the medium was added with quinofumelin (EC_{90}) at a concentration of 1 μg/mL, while an equal amount of dimethyl sulfoxide was added as the control (CK). The incubation continued for another 48 h, followed by filtration and collection of hyphae. Subsequently, Genedenovo Biotechnology Co., Ltd. (Guangzhou, China) performed sequencing on the Illumina platform. Quality control measures were implemented to remove linker sequences and low-quality bases from the original reads in order to obtain clean data readings. The filtered data underwent analysis for base composition and mass distribution to visualize data quality. Based on the gene expression data, we used R (http://www.r-project.org/) for conducting principal component analysis, while the "pheatmap" package was used to generate the clustering heatmap. DESeq2 was applied to analyze group differences based on quantitative expression results. The screening threshold of P value <0.05 and FC≥1.5 or FC≤0.67 was used to identify unigenes with significant differential expression between the two groups using a t-test. Finally, functional enrichment analysis of GO and KEGG pathways was performed on these differentially expressed unigenes.

Metabonomic assay of mycelial growth in *F. graminearum* as affected by quinofumelin

Transcriptome and metabolome samples were obtained from the same treatment group. The widely targeted metabolome analysis was conducted by Metware Biotechnology Co., Ltd. (Wuhan, China). The frozen sample stored at -80°C was thawed on ice. A 400 μL solution (Methanol: Water = 7:3, v/v) containing an internal standard was added to a 20 mg sample and vortexed for 3 min. Subsequently, the sample was sonicated in an ice bath for 10 min and vortexed for 1 min before being placed at -20°C for 30 min. After centrifugation at 12000 rpm for 10 min (4°C). The sediment was removed, followed by another centrifugation of the supernatant at 12000 rpm for 3 min (4°C). A volume of 200 μL aliquots of supernatant was transferred for LC-MS analysis. All samples were acquired using the LC-MS system according to machine orders. The original data file acquired by LC-MS was converted into mzML format using ProteoWizard software. Peak extraction, peak

alignment, and retention time correction were performed by XCMS program.

The identified metabolites were analyzed using MBEole2.0 (https://csbg.cnb.csic.es/mbrole2/index.php) and KEGG (http://www.kegg.jp). PLS-DA analysis was used to identify the differentially accumulated metabolites (DAMs), with a screening threshold of P value<0.05 and FC≥1.5 or FC≤0.67. Each sample was replicated six times for biological consistency.

Recovery assay of quinofumelin-induced mycelial growth inhibition in *F. graminearum*

F. graminearum sensitive strain PH-1 and 9 wild-type strains (*F. graminearum* and *F. asiaticum*), and the PH-1 deletion mutants ΔFgDHODHII, were preincubated on a PDA plate to form mycelial colonies. Mycelial plugs (5 mm in diameter) from the edge of a 3-day-old colony were removed and inoculated onto a CZA plate containing quinofumelin (1 μg/mL) and dihydroorotate, UMP, uridine or uracil at 50 μg/mL, followed by measurement of colony diameters. Three replicates were conducted for each concentration.

Construction of deletion mutant vectors

The deletion mutant of *FgDHODHII* was generated through protoplast transformation, as previously described with some modifications in the transformation procedures[27]. For the transformation process, washed protoplasts were suspended in 160 μL STC and 40 μL SPTC (40% polyethyleneglycol 6000 in STC), along with 2 μg of the aforementioned DNA fragments and 10 μL of heparin (5 mg/mL in STC) to form protoplast suspensions. Subsequently, these mixtures were incubated on ice for 30 min, followed by mixing with 1 mL of SPTC and further incubation at room temperature for 20 min. The resulting suspensions were gently mixed into RM (100 mL) containing 50 μg/mL uridine and poured into plates. After incubating for 24 h at 25°C, the plates were overlaid with SRM containing 50 μg/mL uridine and continuously incubated for an additional 4 days. The putative transformants could be observed growing on SRM. All primers used are listed in SI Appendix, Table 1.

Molecular docking

The binding affinity of quinofumelin with FgDHODHII protein was assessed through molecular docking using AutoDockTools-1.5.7 software. The three-dimensional structure of quinofumelin (PubChem CID: 23160856) used for docking was obtained from PubChem database, while the protein structure models were sourced from the Uniport database. In the docking studies, binding energy was employed as a metric to evaluate the strength of protein-ligand interaction, where lower values indicated higher affinity between proteins and ligands. The resulting docking outcomes were visualized using PyMOL software version 2.5.4.

Surface plasmon resonance (SPR) verification of specific interactions between FgDHODHII and quinofumelin

The cDNA sequence of FgDHODHII was analyzed and codon optimization was performed for the *E. coli* expression system[28-29]. Subsequently, it was ligated into the pCold-9×his-MBP plasmid and the pET-28a plasmid at the NdeI and EcoRI sites within the multiple cloning sites to construct recombinant plasmids: pCold-9×his-MBP-TEV-DHODHII[30], pET-28a (+)-DHODHII and pET-28a (+)-DHODHII$^{124-467}$ (with removal of insoluble fragments) (Supporting Information, Fig. S5).

Plasmid DNA was extracted using the E.Z.N.A Plasmid Extraction DNA Mini Kit I protocol (Omega, China). For protein overexpression, the exacted plasmids were separately transformed into *E. coli* BL21 strain[31]. A single clone obtained from each transformation was used for protein overexpression and purification. Upon reaching an OD600 of 1.0, 0.6 mM isopropyl β-dthiogalactopyranoside (IPTG) was added to induce protein overexpression. Following induction at

16°C for 9 h, cells were harvested, lysed, and purified using a Ni-NTA column (QIAGEN).

The interaction between FgDHODHII and quinofumelin was evaluated using Biacore T200 instrument (GE Healthcare). The CM7 sensor chip was employed for immobilizing 50 μg/mL of purified FgDHODHII protein via amino coupling method at a flow rate of 10 μL/min, utilizing 1×PBS-P+ containing 5% DMSO as running buffer. The desired coupling amount of FgDHODHII protein on the chip surface was targeted to be within the range of 12000-24000 RU. To investigate binding affinity, quinofumelin concentrations were diluted from 3.90625 to 62.5 μM in a constant flow rate running buffer containing 5% DMSO. Following sample injection, a switching buffer was introduced to allow spontaneous dissociation of quinofumelin from FgDHODHII on the chip surface, and this dissociation process was continuously monitored in real time by measuring response values. The affinity value (Kd) was determined through kinetic analysis or steady-state affinity method.

Identification of specific interactions between FgDHODHII and quinofumelin using microscale thermophoresis (MST)

To construct the FgDHODHII-GFP cassette, the FgDHODHII fragment containing the native promoter and ORF (without the stop codon) was amplified. Subsequently, the resulting PCR product was co-transformed with XhoI-digested pYF11 into *E. coli* DH5α as previously reported[32]. The fusion vector was then used to transform PH-1 to obtain the FgDHODHII-GFP strain. The GFP fusion protein was extracted from mycelia. Two Monolith NT.115 standard capillaries were employed for repeated absorption of a specific protein concentration, and placed in positions 1 and 2 of the sample tray in the MonoTemper Monolith NT.115 instrument. Sixteen PCR tubes were prepared, with 10 μL DMSO added to PCR tubes 2-16 and 20 μL of 5000 μM quinofumelin (or phenamacril) dissolved in DMSO added to PCR tube 1. Then, 10 μL of quinofumelin from PCR tube 1 was transferred and thoroughly mixed with PCR tube 2 using a pipette. These steps were repeated for PCR tubes 3–16. Following mixing with PCR tube 16 (discarding the remaining 10 μL), each PCR tube was thoroughly mixed with 190 μL DHODHII-GFP protein, and incubated at room temperature for 30 min. Monolith NT.115 standard capillaries were inserted into each PCR tube to allow solution entry into the capillary. The capillaries 1-16 were subsequently placed in the sample tray of the device and the program was initiated. All measurements were performed using 80% (Auto-detect) Nano-RED. MonoTemper Monolith NT.115 software was used to evaluate the binding affinity between the target protein and quinofumelin using the Kd values and the signal to noise ratio , and the results were combined and analyzed using Mo. Affinity Analysis v2.3 software[33].

Statistical analysis

The data in the study were analyzed using analysis of variance (ANOVA) with the SPSS 14.0 software (SPSS Inc. Chicago, IL, USA). When ANOVA yielded a significant result (p = 0.05), means were compared using Fisher's protected least significant difference (PLSD).

Acknowledgements

This work was supported by the National Key Research and Development Program of China (2022YFD1400100), and the National Natural Science Foundation of China (32072448).

Conflicts of interest

The authors declare no competing interest.

Data availability

Data will be made available on request.

References

1. Lamberth C. Latest Research Trends in Agrochemical Fungicides: Any Learnings for Pharmaceutical Antifungals? *ACS Med. Chem. Lett.* 2022;13(6):895-903. https://10.1021/acsmedchemlett.2c00113.

2. Morton V, Staub T. A Short History of Fungicides. *APSnet Features*. 2008. https://10.1094/APSnetFeature-2008-0308.

3. Lamberth C, Rendine S, Sulzer-Mosse S, Chapter 4 - Agrochemical disease control: The story so far. In *Recent Highlights in the Discovery and Optimization of Crop Protection Products*, Maienfisch, P.; Mangelinckx, S., Eds. Adv Vet Emd-Acad Pr.: 2021; pp 65-85.

4. Duan Y, Xin W, Lu F, et al. Benzimidazole- and QoI-resistance in *Corynespora cassiicola* populations from greenhouse-cultivated cucumber: An emerging problem in China. *Pest. Biochem. Physiol.* 2019;153:95-105. https://https://doi.org/10.1016/j.pestbp.2018.11.006.

5. King K, Bucur D, Ritchie F, et al. Fungicide resistance status and chemical control options for the brassica pathogen *Pyrenopeziza brassicae*. *Plant Pathol.* 2021;70. https://10.1111/ppa.13441.

6. Mao Y, Meng X, Zhang Z, et al. Genetic variation of drug target CYP51 conferring resistance to ergosterol biosynthesis inhibitors in *Botrytis cinerea*, causing lily gray mould. *Ind. Crop. Prod.* 2024;208:117797. https://https://doi.org/10.1016/j.indcrop.2023.117797.

7. Tao X, Zhao H, Xu H, et al. Antifungal Activity and Biological Characteristics of the Novel Fungicide Quinofumelin Against *Sclerotinia sclerotiorum*. *Plant Dis.* 2021;105(9):2567-2574. https://10.1094/PDIS-08-20-1821-RE.

8. Wheeler IE, Hollomon DW, Gustafson G, et al. Quinoxyfen perturbs signal transduction in barley powdery mildew (*Blumeria graminis* f.sp. *hordei*). *Mol. Plant Pathol.* 2003;4(3):177-186. https://https://doi.org/10.1046/j.1364-3703.2003.00165.x.

9. Xiu Q, Bi L, Xu H, et al. Antifungal Activity of Quinofumelin against *Fusarium graminearum* and Its Inhibitory Effect on DON Biosynthesis. *Toxins*. 2021;13(5):348. doi:10.3390/toxins13050348.

10. Bailey TL, Boden M, Buske FA, et al. MEME Suite: tools for motif discovery and searching. *Nucleic Acids Res.* 2009;37(suppl_2):W202-W208. https://10.1093/nar/gkp335.

11. Marchler-Bauer A, Anderson JB, Chitsaz F, et al. CDD: specific functional annotation with the Conserved Domain Database. *Nucleic Acids Res.* 2009;37(suppl_1):D205-D210. https://10.1093/nar/gkn845.

12. Chen C, Chen H, Zhang Y, et al. TBtools: An Integrative Toolkit Developed for Interactive Analyses of Big Biological Data. *Mol. Plant.* 2020;13(8):1194-1202. https://https://doi.org/10.1016/j.molp.2020.06.009.

13. Xiu Q, Bi L, Xu H, et al. Antifungal Activity of Quinofumelin against *Fusarium graminearum* and Its Inhibitory Effect on DON Biosynthesis. *Toxins.* [Online], 2021, p. 348.

14. Chen S-F, Perrella F, Behrens D, et al. Inhibition of Dihydroorotate Dehydrogenase Activity by Brequinar Sodium. *Cancer Res.* 1992;52:3521-7.

15. Mao C, Liu X, Zhang Y, et al. DHODH-mediated ferroptosis defence is a targetable vulnerability in cancer. *Nature*. 2021;593(7860):586-590. https://10.1038/s41586-021-03539-7.

16. Boukalova S, Hubackova S, Milosevic M, et al. Dihydroorotate dehydrogenase in oxidative phosphorylation and cancer. *Biochim. Biophys. Acta-Mol. Basis Dis.* 2020;1866(6):165759. https://https://doi.org/10.1016/j.bbadis.2020.165759.

17. Chen J-J, Jones ME. The cellular location of dihydroorotate dehydrogenase: Relation to de novo biosynthesis of pyrimidines. *Arch. Biochem. Biophys.* 1976;176(1):82-90. https://https://doi.org/10.1016/0003-9861(76)90143-0.

18. Nørager S, Jensen KF, Björnberg O, et al. *E. coli* Dihydroorotate Dehydrogenase Reveals Structural and Functional Distinctions between Different Classes of Dihydroorotate Dehydrogenases. *Structure*. 2002;10(9):1211-1223. https://https://doi.org/10.1016/S0969-2126(02)00831-6.

19. Dorasamy MS, Choudhary B, Nellore K, et al. Dihydroorotate dehydrogenase Inhibitors Target c-Myc and Arrest Melanoma, Myeloma and Lymphoma cells at S-phase. *J. Cancer*. 2017;8(15):3086-3098. https://10.7150/jca.14835.

20. Alves C, Silva J, Roitberg A. Insights into the Mechanism of Oxidation of Dihydroorotate to Orotate Catalysed by Human Class 2 Dihydroorotate Dehydrogenase: A QM/MM Free Energy Study. *Phys. Chem. Chem. Phys.* 2015;17. https://10.1039/C5CP02016F.

21. Olaru A, Bala C, Jaffrezic-Renault N, et al. Surface Plasmon Resonance (SPR) Biosensors in Pharmaceutical Analysis. *Crit. Rev. Anal. Chem.* 2015;45(2):97-105. https://10.1080/10408347.2014.881250.

22. Guo X. Surface plasmon resonance based biosensor technique: A review. *J. Biophotonics*. 2012;5(7):483-501. https://https://doi.org/10.1002/jbio.201200015.

23. Piliarik M, Vaisocherová H, Homola J, Surface Plasmon Resonance Biosensing. In *Biosensors and Biodetection*, Rasooly, A.; Herold, K. E., Eds. Humana Press: Totowa, NJ, 2009; pp 65-88.

24. Wang Y, Hekimi S. Understanding Ubiquinone. *Trends Cell Biol.* 2016;26(5):367-378. https://https://doi.org/10.1016/j.tcb.2015.12.007.

25. Higashimura N, Hamada A, Ohara T, et al. The target site of the novel fungicide quinofumelin, *Pyricularia oryzae* class II dihydroorotate dehydrogenase. *J. Pestic. Sci.* 2022;47(4):190-196. https://10.1584/jpestics.D22-027.

26. Cleland WW. The kinetics of enzyme-catalyzed reactions with two or more substrates or products: III. Prediction of initial velocity and inhibition patterns by *Biochim. Biophys. Acta*. 1963;67:188-196. https://https://doi.org/10.1016/0926-6569(63)90227-X.

27. Zhang L, Li B, Zhang Y, et al. Hexokinase plays a critical role in deoxynivalenol (DON) production and fungal development in *Fusarium graminearum*. *Mol. Plant Pathol.* 2016;17(1):16-28. https://https://doi.org/10.1111/mpp.12258.

28. Kyriakopoulos S, Kontoravdi C. Analysis of the landscape of biologically-derived pharmaceuticals in Europe: Dominant production systems, molecule types on the rise and approval trends. *Eur. J. Pharm. Sci.* 2013;48(3):428-441. https://https://doi.org/10.1016/j.ejps.2012.11.016.

29. Yang D, Prabowo CPS, Eun H, et al. *Escherichia coli* as a platform microbial host for systems metabolic engineering. *Essays Biochem.* 2021;65(2):225-246. https://10.1042/EBC20200172.

30. Fang K, Li Y, Yin X, et al. High-Level Prokaryotic Expression and Purification of Death Domain Superfamily with MBP Tag. *Clin. Lab.* 2018;64(4):467-475. https://10.7754/clin.lab.2017.170922.

31. Zhu L, Zhang X, Chang L, et al. Molecular cloning, prokaryotic expression and promoter analysis of squalene synthase gene from *Schizochytrium Limacinum*. *Appl. Biochem. Microbiol.* 2014;50(4):411-419. https://10.1134/S0003683814040140.

32. Tang G, Chen A, Dawood DH, et al. Capping proteins regulate fungal development, DON-toxisome formation and virulence in *Fusarium graminearum*. *Mol. Plant Pathol.* 2020;21(2):173-187. https://https://doi.org/10.1111/mpp.12887.

33. Rotem O, Nesper J, Borovok I, et al. An Extended Cyclic Di-GMP Network in the Predatory Bacterium *Bdellovibrio bacteriovorus*. *J. Bacteriol.* 2015;198(1):127-137. https://10.1128/jb.00422-15.

Figures:

Fig. 1 Analysis of transcriptome sequencing data in *F. graminearum* PH-1 treated with quinofumelin.

a Bar chart illustrating the comparison of differentially expressed genes between EC_{90} treatments and the control.

b Volcano plot depicting up-regulated DEGs as red scattered dots and down-regulated DEGs as blue scattered dots.

c Cluster heat maps displaying gene relative expression values using RNA-seq data scale-standardized values.

d Bubble map presenting the results of GO enrichment analysis for DEGs.

e Bubble map showcasing the findings of KEGG enrichment analysis for DEGs.

Fig.2 Difference analysis and enrichment analysis of metabolome data in *F. graminearum* PH-1 treated with quinofumelin.

a Bar chart illustrating the number of differential accumulation metabolites (DAMs) quantity in experimental groups (EC_{90}) and control groups (CK) in positive ion mode.

b Volcanic map of all metabolites in positive ion mode. The red scatter points represent up-regulated DAMs, while the blue scatter points represent down-regulated DAMs.

c Classification and proportion of DAMs.

d Bubble diagram of differential accumulation metabolite KEGG enrichment pathway.

e Pyrimidine *de novo* biosynthesis pathway in *Fusarium graminearum*. The left box plots represent the relative content of 8 metabolite samples, while the right box represents the relative content of 6 gene samples. The color gradient from navy blue to firebrick red indicates a progression from low to high content.

Fig. 3 Phylogenic tree of DHODHII proteins. The phylogenetic tree was constructed based on the amino acid sequences of DHODHII homologous protein with Mega X using the neighbor-joining method. The bootstrap values from 1000 replications are indicated on the branches. Motif pattern information was generated using the MEME suite12, while functional domain information and protein coordinates were obtained through CD-search. The final phylogenetic tree was visualized using TBtools. FgDHODHII was highlighted in red. The amino acid sequence of *DHODHII* from *Alternaria alternata* (AA0117_g542), *Aspergillus nidulans* (ANIA_05909), *Aspergillus oryzae* (AO1008_05965), *Blumeria graminis* (BLGH_00861), *Botrytis cinerea* (Bcin15g04150), *Botrytis elliptica* (BELL_0162g00150), *Colletotrichum asianum* (GQ607_007053), *Colletotrichum fioriniae* (CFIO01_03831), *Colletotrichum higginsianum* (CH063_10143), *Corynespora cassiicola* (BS50DRAFT_576390), *Erysiphe necator* (EV44_g2092), *Erysiphe pulchra* (EPUL_004094), *Fusarium euwallaceae* (BHE90_002825), *Fusarium floridanum* (CEP51_012005), *Fusarium fujikuroi* (FFMR_05040), *Fusarium graminearum* (FGSG_09678), *Fusarium nygamai* (FNYG_10990), *Fusarium odoratissimum* (FOIG_08270), *Fusarium oxysporum* (FOXG_08390), *Fusarium pseudograminearum* (FPSE_04283), *Fusarium solani* (NechaG15121), *Fusarium verticillioides* (FVEG_06288), *Magnaporthe oryzae* (MGG_08814), *Neurospora crassa* (NCU06532), *Oidium neolycopersici* (OnM2_089032), *Pestalotiopsis fici* (PFICI_04984), *Podospora anserina* (PODANS_6_7920), *Puccinia graminis* (PGTG_16739), *Puccinia triticina* (PTTG_02070), *Rhizoctonia solani* (RSOLAG22IIIB_08327), *Schizosaccharomyces pombe* (SPAC57A10.12c), *Ustilaginoidea virens* (UVI_02052880), *Verticillium alfalfae* (VDBG_01322),

Verticillium dahliae (VDAG_07935), and *Zymoseptoria tritici* (Mycgr3G72548) were accessed in EnsemblFungi database.

Fig. 4 Recovery test of mycelial growth suppressed by quinofumelin.

All strains were incubated on CZA plates at 25°C for 3 days. *F. graminearum* strains PH-1, 512E-8, SX2117, XY-4, and R10. The left image shows the colony morphology, while the right image is a bar chart of colony diameters.

Fig. 5 Mycelial growth of FgDHODHII deletion mutants on CZA plates.

a Mycelial growth of the FgDHODHII deletion mutants and the parental strain was observed in the presence or absence of 50 μg/mL uridine.

b Recovery of mycelial growth of the FgDHODHII deletion mutants was observed in the presence of 50 μg/mL dihydroorotate, UMP, uridine or uracil. All strains were incubated at 25°C for 3 days.

Fig. 6 Validation and analysis of quinofumelin's binding affinity to FgDHODHII.

a Three-dimensional model of the wild-type FgDHODHII are depicted, with an enlarged view highlighting the binding site for quinofumelin on the corresponding FgDHODHII models.

b The SPR response (RU) analysis and fitting results demonstrate the interaction between quinofumelin and FgDHODHII.

c Microscale thermophoresis (MST) analysis to detect the binding of quinofumelin and FgDHODHII.

603 **Tables:**

604 **Table 1 Primers used in the study**

Primer	Sequence (5'-3')	Use
FgDHODHII-UF	GGCAGTGAAAGTCTTGTTCAAG	PCR primers to amplify FgDHODHII upstream fragment
FgDHODHII-UR	GCTCCTTCAATATCATCTTCTGTGGC TGGGAAGTAATGCTGGG	
FgDHODHII-DF	GAGACAATACCGGAAGGAACAC ATGCTATAGCAAGCAACA	PCR primers to amplify FgDHODHII downstream fragment
FgDHODHII-DR	AAACTTAACAAATCATCTTTGCC	
SS-F	ACAGAAGATGATATTGAAGGAGC	PCR primers to amplify Hph-Hsv-tk fragment
SS-R	GAGACAATACCGGAAGGAA	
FgDHODHII-YZ-F	TTTGCCCGATCTCTTGGTCT	PCR primers to verify FgDHODHII
FgDHODHII-YZ-R	AACCACCAGTCTCCATGAGG	
FgDHODHII-GFP-F	CTCATCACCATCACCATCACAT GTCTGCCGCTCTCCTACG	Constructed FgDHODHII-GFP fusion vector
FgDHODHII-GFP-R	AGCTCCTCGCCCTTGCTCACCC TCGAATTCTTCACACCAC	
T7	TAATACGACTCACTATAGG	
T7t	CCGCTAGTTATTGCTCAGC	
pET-28a-F	CCTGGTGCCGCGCGGCAGCCATATGCTGG CTGTCAATGTTTTTGGAACAG	PCR primers to construct FgDHODHII expression vector
pET-28a-R	AAGCTTGTCGACGGAGCTCGAATTCCTAT TTTAACTCCTGCTTGATCCTG	
pCold-F	GTAAAGCACGCCATATCGC	
pCold-R	CCAAATGGCAGGGATCTTAG	

605

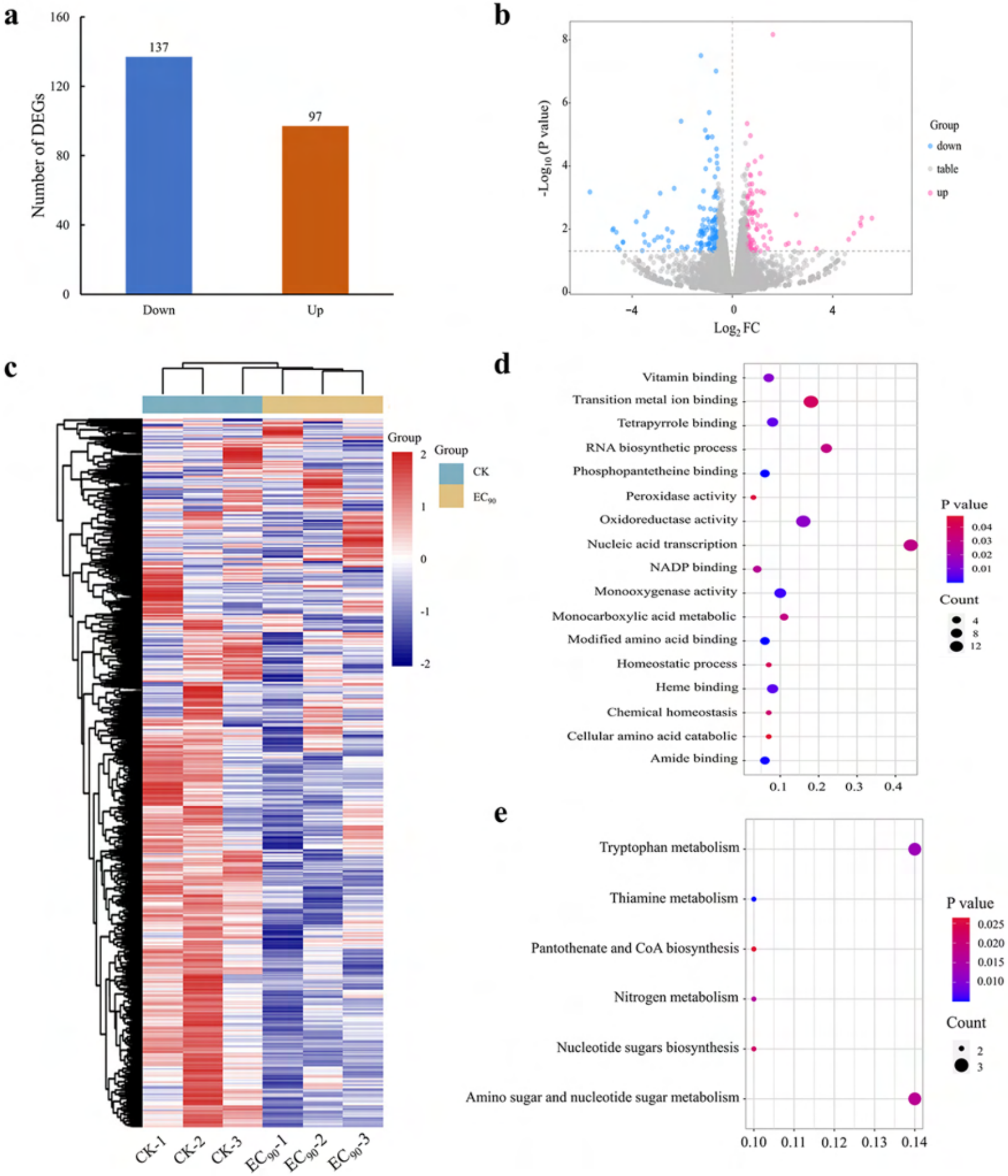
a
Number of DEGs
160
120
80
40
0
137
97
Down
Up
b
-Log10 (P value)
Log2 FC
Group
down
table
up
c
Group
CK
EC90
CK-1
CK-2
CK-3
EC90-1
EC90-2
EC90-3
d
Vitamin binding
Transition metal ion binding
Tetrapyrrole binding
RNA biosynthetic process
Phosphopantetheine binding
Peroxidase activity
Oxidoreductase activity
Nucleic acid transcription
NADP binding
Monooxygenase activity
Monocarboxylic acid metabolic
Modified amino acid binding
Homeostatic process
Heme binding
Chemical homeostasis
Cellular amino acid catabolic
Amide binding
P value
Count
e
Tryptophan metabolism
Thiamine metabolism
Pantothenate and CoA biosynthesis
Nitrogen metabolism
Nucleotide sugars biosynthesis
Amino sugar and nucleotide sugar metabolism
P value
Count

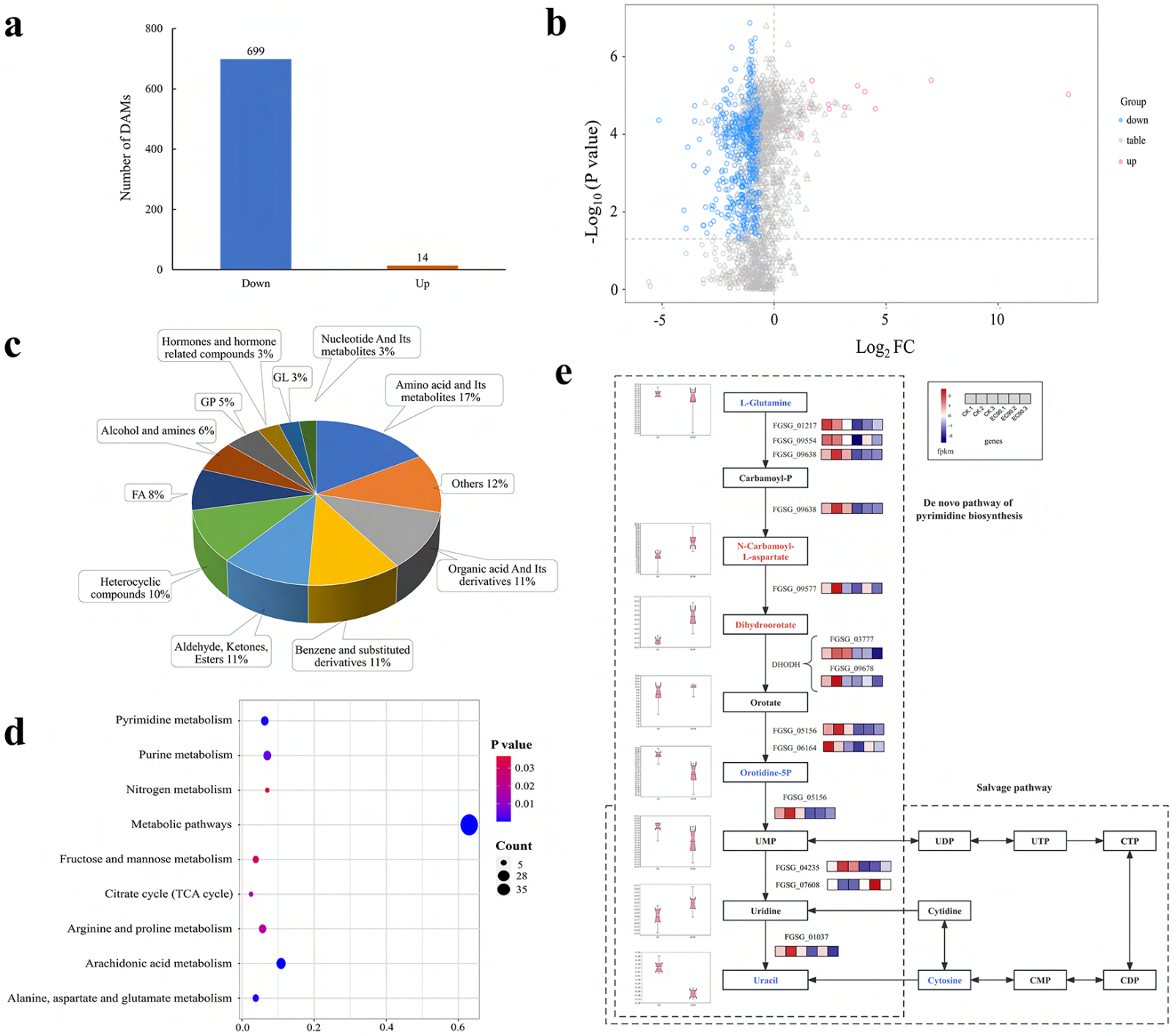
a
Number of DAMs
800
600
400
200
0
699
14
Down
Up
b
-Log10 (P value)
Log2 FC
Group
down
table
up
c
Hormones and hormone related compounds 3%
Nucleotide And Its metabolites 3%
GL 3%
GP 5%
Amino acid and Its metabolites 17%
Alcohol and amines 6%
Others 12%
FA 8%
Organic acid And Its derivatives 11%
Heterocyclic compounds 10%
Aldehyde, Ketones, Esters 11%
Benzene and substituted derivatives 11%
d
Pyrimidine metabolism
Purine metabolism
Nitrogen metabolism
Metabolic pathways
Fructose and mannose metabolism
Citrate cycle (TCA cycle)
Arginine and proline metabolism
Arachidonic acid metabolism
Alanine, aspartate and glutamate metabolism
P value
0.03
0.02
0.01
Count
5
28
35
e
L-Glutamine
FGSG_01217
FGSG_09554
FGSG_09638
Carbamoyl-P
FGSG_09638
N-Carbamoyl-L-aspartate
FGSG_09577
Dihydroorotate
FGSG_03777
DHODH
FGSG_09678
Orotate
FGSG_05156
FGSG_06164
Orotidine-5P
FGSG_05156
UMP
FGSG_04235
FGSG_07608
Uridine
FGSG_01037
Uracil
De novo pathway of pyrimidine biosynthesis
Salvage pathway
UDP
UTP
CTP
Cytidine
Cytosine
CMP
CDP
fpkm
genes

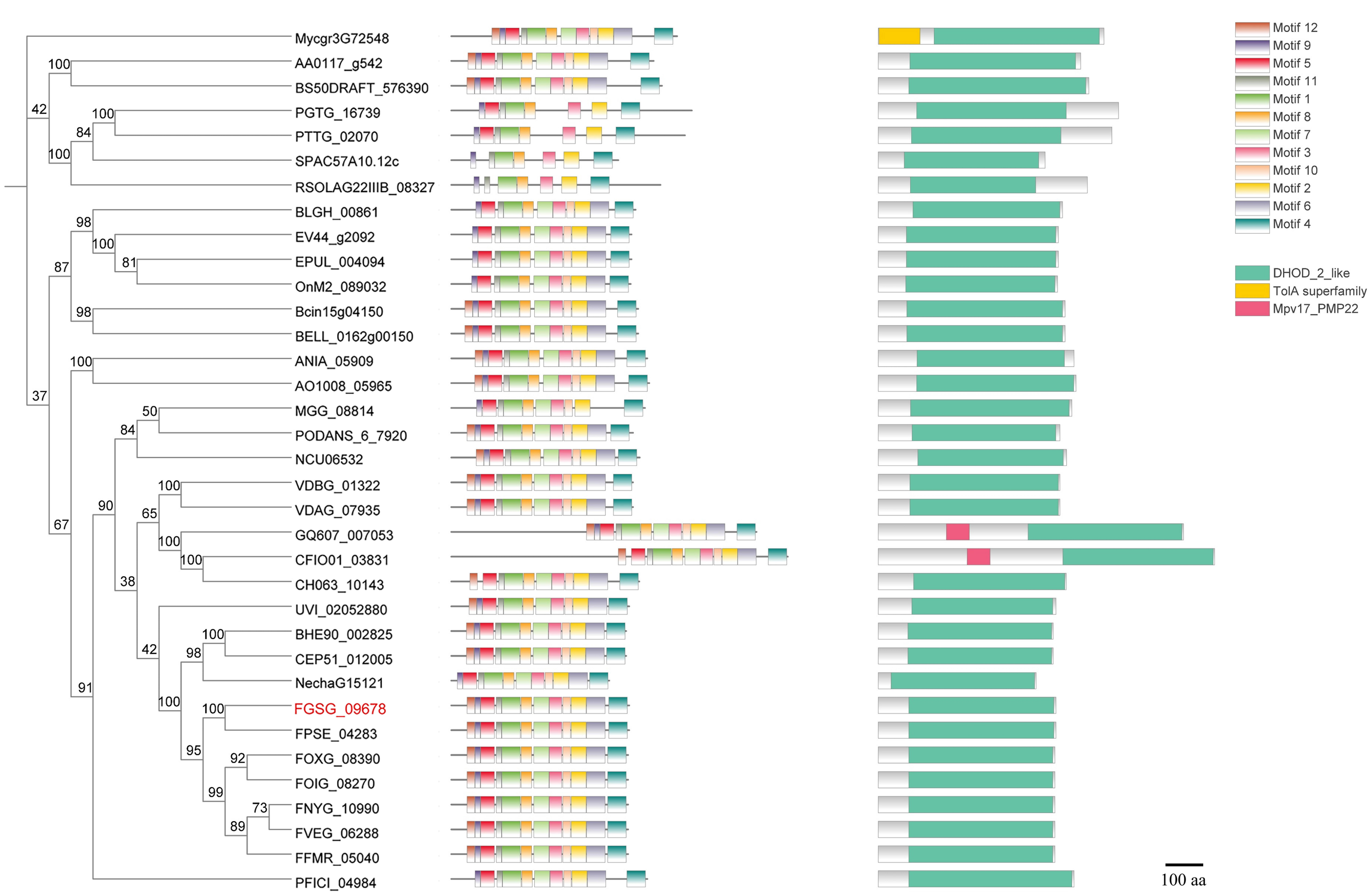
Mycgr3G72548
AA0117_g542
BS50DRAFT_576390
PGTG_16739
PTTG_02070
SPAC57A10.12c
RSOLAG22IIIB_08327
BLGH_00861
EV44_g2092
EPUL_004094
OnM2_089032
Bcin15g04150
BELL_0162g00150
ANIA_05909
AO1008_05965
MGG_08814
PODANS_6_7920
NCU06532
VDBG_01322
VDAG_07935
GQ607_007053
CFIO01_03831
CH063_10143
UVI_02052880
BHE90_002825
CEP51_012005
NechaG15121
FGSG_09678
FPSE_04283
FOXG_08390
FOIG_08270
FNYG_10990
FVEG_06288
FFMR_05040
PFICI_04984
Motif 12
Motif 9
Motif 5
Motif 11
Motif 1
Motif 8
Motif 7
Motif 3
Motif 10
Motif 2
Motif 6
Motif 4
DHOD_2_like
TolA superfamily
Mpv17_PMP22
100 aa

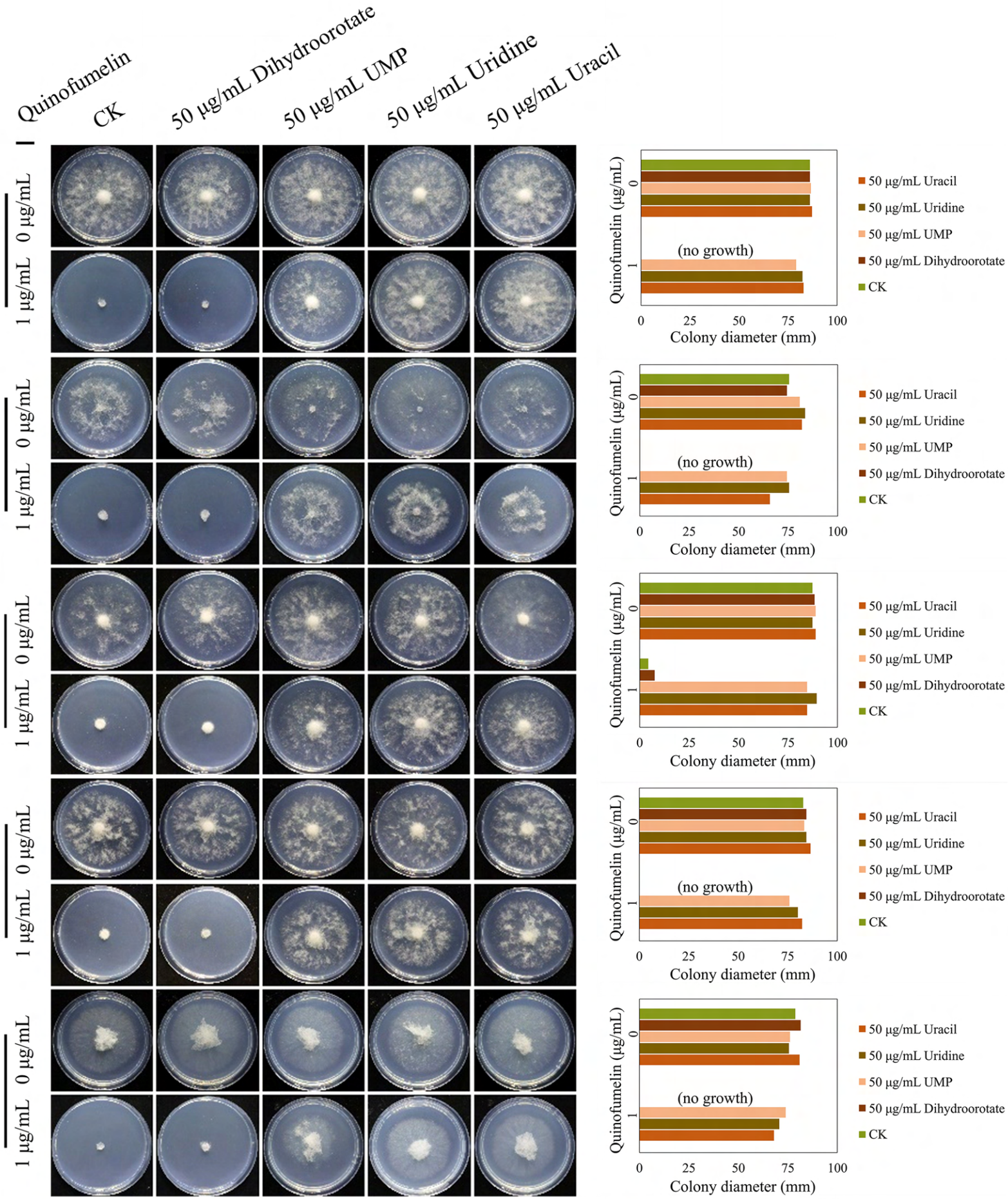
Quinofumelin
CK
50 μg/mL Dihydroorotate
50 μg/mL UMP
50 μg/mL Uridine
50 μg/mL Uracil
PH-1
512E-8
SX2117
XY-4
R10
0 μg/mL
1 μg/mL
(no growth)
Quinofumelin (μg/mL)
Colony diameter (mm)
0
25
50
75
100
50 μg/mL Uracil
50 μg/mL Uridine
50 μg/mL UMP
50 μg/mL Dihydroorotate
CK

a

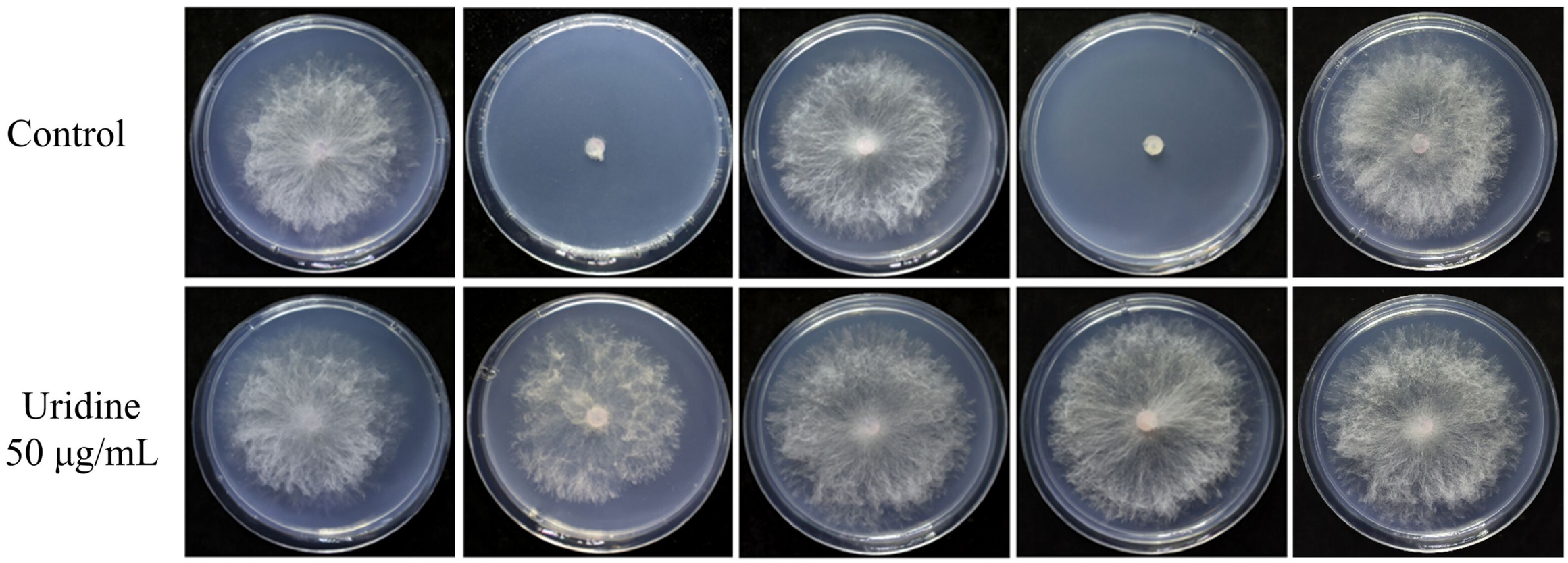
PH-1
ΔFgDHODHII-1
ΔFgDHODHII-1-C
ΔFgDHODHII-2
ΔFgDHODHII-2-C
Control
Uridine
50 μg/mL

b

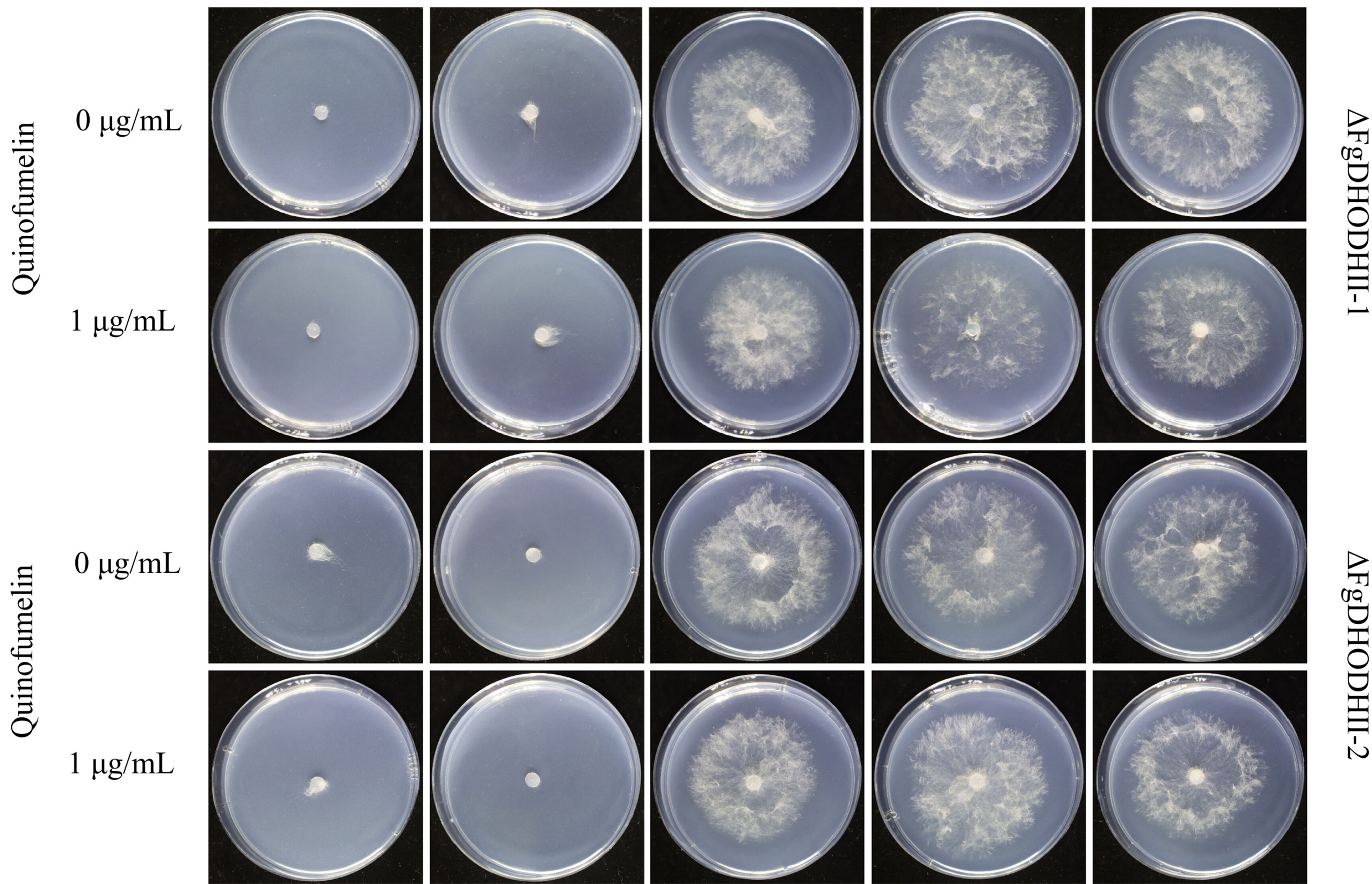
Control
50 μg/mL Dihydroorotate
50 μg/mL UMP
50 μg/mL Uridine
50 μg/mL Uracil
Quinofumelin
0 μg/mL
1 μg/mL
ΔFgDHODHII-1
Quinofumelin
0 μg/mL
1 μg/mL
ΔFgDHODHII-2

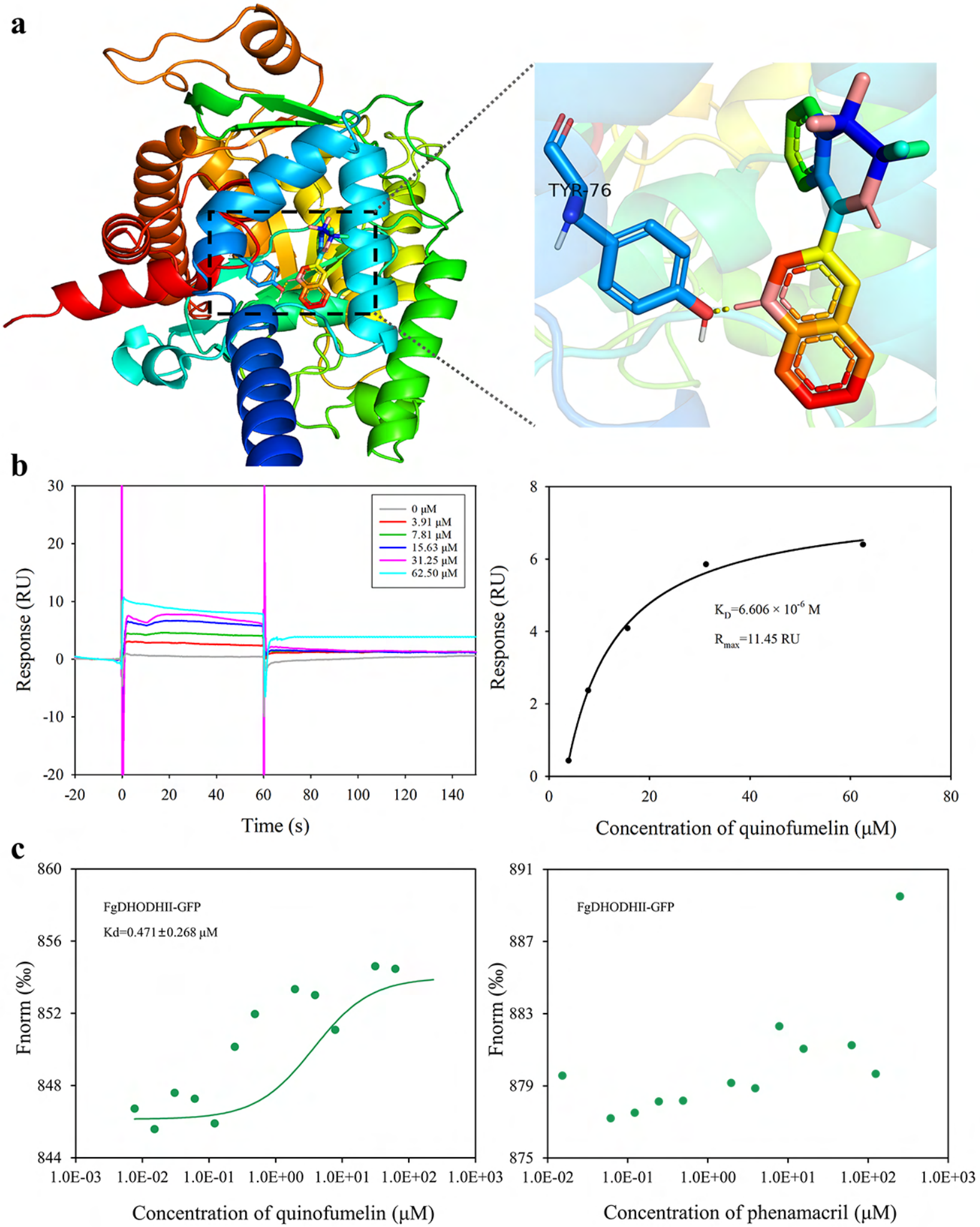
a
TYR-76
b
0 μM
3.91 μM
7.81 μM
15.63 μM
31.25 μM
62.50 μM
Response (RU)
Time (s)
K_D=6.606 × 10^{-6} M
R_{max}=11.45 RU
Response (RU)
Concentration of quinofumelin (μM)
c
FgDHODHII-GFP
Kd=0.471±0.268 μM
Fnorm (‰)
Concentration of quinofumelin (μM)
FgDHODHII-GFP
Fnorm (‰)
Concentration of phenamacril (μM)